



## Characterization of levan produced by a *Paenibacillus* sp. isolated from Brazilian crude oil

Carlos M.N. Mendonça<sup>a,b</sup>, Rodrigo C. Oliveira<sup>a</sup>, Rominne K.B. Freire<sup>a</sup>, Anna C.M. Piazzentin<sup>a</sup>, Wellison A. Pereira<sup>a</sup>, Eduardo J. Gudiña<sup>c</sup>, Dmitry V. Evtuguin<sup>b</sup>, Attilio Converti<sup>d</sup>, João H.P. M. Santos<sup>a</sup>, Cláudia Nunes<sup>b</sup>, Lígia R. Rodrigues<sup>c,1</sup>, Ricardo P.S. Oliveira<sup>a,\*,1</sup>

<sup>a</sup> Department of Biochemical and Pharmaceutical Technology, University of São Paulo, 05508-000 São Paulo, Brazil

<sup>b</sup> CICECO, Aveiro Institute of Materials, Department of Chemistry, University of Aveiro, 3810-193 Aveiro, Portugal

<sup>c</sup> CEB, Centre of Biological Engineering, University of Minho, 4710-057 Braga, Portugal

<sup>d</sup> Department of Civil, Chemical and Environmental Engineering, Pole of Chemical Engineering, University of Genoa, Via Opera Pia 15, 16145 Genoa, Italy

### ARTICLE INFO

#### Keywords:

Levan  
Physicochemical characterization  
Thermomechanical stability

### ABSTRACT

A levan-type fructooligosaccharide was produced by a *Paenibacillus* strain isolated from Brazilian crude oil, the purity of which was 98.5% after precipitation with ethanol and dialysis. Characterization by FTIR, NMR spectroscopy, GC-FID and ESI-MS revealed that it is a mixture of linear  $\beta(2 \rightarrow 6)$  fructosyl polymers with average degree of polymerization (DP) of 18 and branching ratio of 20. Morphological structure and physicochemical properties were investigated to assess levan microstructure, degradation temperature and thermomechanical features. Thermal Gravimetric Analysis highlighted degradation temperature of 218 °C, Differential Scanning Calorimetry (DSC) glass transition at 81.47 °C, and Dynamic Mechanical Analysis three frequency-dependent transition peaks. These peaks, corresponding to a first thermomechanical transition event at 86.60 °C related to the DSC endothermic event, a second at 170.9 °C and a third at 185.2 °C, were attributed to different glass transition temperatures of oligo and polyfructans with different DP. Levan showed high morphological versatility and technological potential for the food, nutraceutical, and pharmaceutical industries.

### 1. Introduction

Fructooligosaccharides (FOS), also known as oligofructans, are a group of oligosaccharides composed of fructosyl oligomers with different chemical structures and degrees of polymerization (DP) [1,2]. Capable of resisting the digestion process in the upper gastrointestinal tract, FOS are known to stimulate the growth of specific endogenous probiotics of gut microbiota (e.g. *Bifidobacterium* spp. and *Lactobacillus* spp.) [3], while suppressing the growth of pathogens [2,4]. Their role in boosting the immune system and reducing the risks of gastrointestinal infection and inflammation, as well as their therapeutic effects against inflammatory bowel disease, obesity-related metabolic disorders, diabetes and diarrhea, has been demonstrated in a significant number of experimental studies [4–7]. Further beneficial effects deriving from the direct interactions of these non-digestible oligosaccharides with host intestinal cells have also been described, in accordance with their

recognition as soluble dietary fibers [8]. Based on their natural origin and remarkable health benefits, FOS are generally recognized as safe (GRAS) by the Food and Drug Administration (FDA) and other regulatory agencies around the world [9,10].

Levan-based FOS gained considerable interest in food and nutraceutical industries due to their biocompatibility, biodegradability, anti-inflammatory and anticarcinogenic effects, bioactivity profiles and organoleptic properties [11,12]. Produced by a small number of plant species as non-structural storage carbohydrates and by a wide range of microorganisms as exopolysaccharides (EPS), these fructose homopolymers exhibit a main glycosidic chain composed of repeating fructofuranosyl units linked mainly or exclusively by  $\beta(2 \rightarrow 6)$  glycosidic bonds. Although predominantly linear, especially levans with high DP may have some degree of branching through  $\beta(2 \rightarrow 1)$  fructosyl-fructose bonds [13]. Given the current market demand and growing industrial interest in such biopolymers, large-scale microbial production has been

\* Corresponding author.

E-mail address: [rpsolive@usp.br](mailto:rpsolive@usp.br) (R.P.S. Oliveira).

<sup>1</sup> Lígia R. Rodrigues and Ricardo P. S. Oliveira shared last co-author.

<https://doi.org/10.1016/j.ijbiomac.2021.07.036>

Received 12 April 2021; Received in revised form 4 June 2021; Accepted 3 July 2021

Available online 8 July 2021

0141-8130/© 2021 Elsevier B.V. All rights reserved.

proposed as an alternative to the current industrial production from plant raw materials [14].

The main current drawback of large-scale biotech production of oligo and polyfructans is the high cost of unit operations required to achieve the desired product yield as well as the required levels of purity and safety standards. Therefore, the development of low-cost upstream and downstream operations is of paramount importance to increase the techno-economic feasibility of these processes, especially in the field of bioactive food grade dietary fibers. To minimize the purification steps and ensure a cost-effective production process, the use of a low-complexity, low-cost nutrient-based culture medium is required. Moreover, the search for new levan-producing microorganisms, which can grow under such severe nutritional conditions but provide high production yields, is of particular interest. Despite the growing number of articles reporting the identification of novel levan-producing microbial strains, there is a paucity of studies devoted to the complete physicochemical characterization of the complex biopolymer blends typically obtained. Since FOS application in the food (*i.e.* food thickeners, edible films and coatings, prebiotics, among others), medical, pharmaceutical and cosmetic (*i.e.* glazing agents) sectors strongly depends on structural characteristics such as molecular weight, DP and ramification degree, studies are needed to evaluate the physicochemical properties of these blends in order to allow their proper commercial use [15]. In particular, the study of FOS thermogravimetric, thermomechanical, and morphological properties is considered essential given their growing applications in emerging products in the field of materials science and biopolymers.

In the present work, the production of bacterial oligo and polyfructan by a *Paenibacillus* strain isolated from Brazilian crude oil was investigated in a low-complexity, low-cost Mineral Salt Solution supplemented with sucrose and ammonium nitrate as carbon and nitrogen sources, respectively. The oligo and polyfructan mixture produced after 24 h in shake flasks at 140 rpm and 40 °C was purified by precipitation with ethanol and dialysis and then characterized in terms of sugar composition, type of bonds, as well as polymerization and branching degrees, using FTIR, NMR, GC-FID, GC-MS and ESI-MS. Finally, its microstructure, thermal stability and thermomechanical features were investigated by X-ray Diffraction Analysis, SEM, TGA, DSC and DMA, taking into consideration its main potential applications in different commercial sectors.

## 2. Materials and methods

### 2.1. Microorganism

The bacterial strain #210, isolated from heavy crude oil samples obtained from a Brazilian oil well (Potiguar, Northeast Brazil), was used in this work. The reservoir is characterized by alternated oil and water sand layers, with average porosity of 25%, permeability of 50 mD, pressure of 398–440 psi and temperature of 40 °C. The oil is paraffinic, with a high pour point and its density, viscosity, and American Petroleum Institute (API) gravity are 0.90 g L<sup>-1</sup>, 73.91 mPa s, and 25.5°, respectively. The Saturate, Aromatic, Resin and Asphaltene (SARA) analysis revealed that this oil contains 55% of saturates (*n*-alkanes ranging from C14 to C32), 18% of aromatics, 19% of resins, and 8% of asphaltenes [16].

Crude oil samples were collected at depths of 300–400 m in sterile bottles and stored at room temperature until use. For isolation of microorganisms, two different methods were used as described by Gudiña et al. [16]. Direct isolation was performed by serially diluting crude oil samples, which were plated on different solid culture media and incubated under either aerobic or anaerobic conditions at 40 °C. Enrichment cultures were prepared in 500 mL glass bottles containing 200 mL of different culture media. Crude oil samples (5 mL) were transferred to the bottles and incubated at 40 °C for one month under either aerobic or anaerobic conditions. To isolate bacterial strains, samples (200 µL) of

the enrichment cultures were periodically spread on agar plates, which were incubated at 40 °C under either aerobic or anaerobic conditions. In both cases, after incubation, morphologically distinct colonies were re-isolated by transfer to fresh agar plates at least three times to obtain pure cultures. Pure cultures were stored at -80 °C in LB medium containing glycerol (20%, v/v).

All the isolates were evaluated for their production of different biomolecules, including biosurfactants and bioemulsifiers, as described elsewhere [16]. The isolate #210 was selected since it proved to be a promising emulsifier producer. It was then characterized by 16S rRNA gene sequencing after partial amplification by PCR. The resulting sequences were compared using the nucleotide blast (BLASTn) network service at the GenBank database of the National Center for Biotechnology Information (NCBI) (<http://www.ncbi.nlm.nih.gov>). Based on the results obtained, the bacterial isolate was classified as *Paenibacillus* sp. #210. The 16S rRNA gene sequence was deposited in GenBank under the accession number MW577094.

### 2.2. Levan production

#### 2.2.1. Culture medium and growth conditions

Levan production was carried out by culturing *Paenibacillus* sp. #210 in Mineral Salt Solution (MSS) having the following composition (g·L<sup>-1</sup>): NaCl 10.0; Na<sub>2</sub>HPO<sub>4</sub> 5.0; NH<sub>4</sub>NO<sub>3</sub> 2.0; KH<sub>2</sub>PO<sub>4</sub> 2.0; MgSO<sub>4</sub>·7H<sub>2</sub>O 0.2 and enriched with sucrose 10.0. To prepare the pre-inoculum, the isolate was initially grown at 37 °C for 96 h on MSS agar plates. A single bacterial colony was subsequently transferred to 250-mL Erlenmeyer flasks containing 100 mL of liquid MSS medium and incubated at 40 °C in an orbital shaker at 180 rpm for 12 h. The inoculum was prepared by resuspending freshly grown pre-inoculum biomass, previously centrifuged at 3000 rpm for 10 min, in fresh MSS medium contained in 50-mL Falcon tubes up to a final absorbance of 0.400 at 600 nm. The inoculum (100 mL) was added to 1-L Erlenmeyer flask containing 400 mL of MSS medium and further incubated at 40 °C and 140 rpm for 24 h. The medium was sterilized in autoclave at 121 °C for 30 min and equilibrated at 40 °C before inoculation. Cultivations were carried out in triplicate.

#### 2.2.2. Analytical determinations

Microbial growth was continuously monitored by measurements of optical density at 600 nm (Dynamica Halo Vis-10, Clayton, Australia), whose values were converted into cell concentration using a calibration curve of optical density vs biomass dry weight. Aliquots (1 mL) were collected approximately every 30 min during the first 11 h and at the end of cultivation (24 h). The dissolved O<sub>2</sub> level and pH were monitored in real time (in one of the three parallel batch cultivations) using a pO<sub>2</sub> sensor (325/12-VP-HM-Clark, Hamilton, Bonaduz, Switzerland) and a pH sensor (225/12-VP-HM, Hamilton) coupled with a micro-DCU platform and data acquisition MFCS/DA 3.0 system (Sartorius Stedim Systems, Guxhagen, Germany).

### 2.3. Levan purification

After cultivation, biomass was removed from the medium by centrifugation at 4470 g for 20 min at 25 °C, and the cell-free supernatant mixed with three volumes of ethanol, incubated overnight at -20 °C and centrifuged again at 4470 g for 20 min at 4 °C. The EPS-containing pellet was subsequently dissolved in a minimum volume of demineralized water and dialyzed using a semipermeable regenerated cellulose membrane (Orange Scientific, Braine L'Alleud, Belgium) with a cut-off of 6000–8000 Da and width of 25 mm. Dialysis was performed using 4.0 L of deionized water for 4 cycles of 2 h and a final one of 12 h at 4 °C, and the dialysate subsequently filtered through a filter with 0.45-µm pore diameter, frozen and lyophilized using a freeze dryer (L101, Liobras, São Carlos, SP, Brazil).

## 2.4. Levan characterization

### 2.4.1. Elemental analysis

The freeze-dried dialyzed EPS and a crude freeze-dried sample were analyzed for total C, H, N, and S contents using a Truspec-Micro CHNS 630-200-200 elemental analyzer (Leco, St. Joseph, MI, USA). Temperatures of the combustion furnace and the afterburner were 1075 and 850 °C, respectively. Infrared absorption was used for C, H and S determinations, while thermal conductivity for N. Each sample (2.0 ± 0.2 mg) was analyzed in triplicate.

### 2.4.2. Fourier transform infrared spectroscopy

Fourier Transform Infrared Spectroscopy (FTIR) profiles of freeze-dried dialyzed EPS, as well as glucose and fructose standards, were recorded using a FT Raman 100/S spectrometer (Bruker, Billerica, MA, USA) in mid-IR mode, equipped with a Universal Attenuated Total Reflectance sampling device containing diamond/ZnSe crystal. The pressure applied to squeeze powdered samples towards the diamond was approximately 148 ± 1 N. Spectra were scanned at room temperature in transmittance mode over a wavenumber range from 4000 to 50 cm<sup>-1</sup>, with a scan speed of 0.20 cm·s<sup>-1</sup> and 30 accumulations at a resolution of 4 cm<sup>-1</sup>. Triplicates of each sample were averaged to obtain an average spectrum. A background spectrum of air was scanned under the same instrumental conditions before each series of measurements. The acquired spectra were processed with the Spectrum software version 6.3.2 (Perkin Elmer, Shelton, CT, USA).

### 2.4.3. Sugar analyses

**2.4.3.1. Neutral sugar content.** The glycosidic composition of the freeze-dried dialyzed EPS was assessed by analysing the alditol acetates of sugars [17]. The analysis included two steps: hydrolysis of all oligo and polysaccharide glycosidic bonds, followed by reduction and acetylation. Briefly, freeze-dried dialyzed EPS samples (2 mg) were pre-hydrolyzed with 72% (w/w) sulfuric acid (200 µL) for 3 h at room temperature. Samples were then further hydrolyzed with 1.0 M sulfuric acid at temperatures of 70 or 100 °C for 10, 20, 30, 40, 50, 60, and 150 min. A 1 mg·mL<sup>-1</sup> 2-deoxyglucose aqueous solution (200 µL) was added to the obtained hydrolyzate as an internal standard, and the monosaccharides were reduced with 100 µL of 15% (w/v) sodium borohydride in 3 M NH<sub>3</sub> at 30 °C for 1 h. Excess borohydride was then removed by adding glacial acetic acid (100 µL), and the reduced monosaccharides were acetylated with acetic anhydride (1.0 mL) and 1-methylimidazole (3.0 mL) for 30 min at 30 °C. The solution was then treated with deionized water (3.0 mL) to decompose the excess of acetic anhydride, and the alditol acetates were extracted with dichloromethane (2.5 mL). The dichloromethane phase was washed twice with deionized water (3.0 mL) and evaporated to dryness. Samples were then injected into a gas chromatograph (Clarus 400, Perkin Elmer, Norwalk, CT, USA) with flame ionization detector (CG-FID), equipped with a DB-225 column (30 m long, 0.25 mm in diameter and 0.5 µm thick). The temperature program used for the analysis of alditol acetates was as follows. The temperature was initially set at 200 °C, increased to 220 °C at a heating rate of 40 °C·min<sup>-1</sup> and kept at this temperature for 7 min. Then, it was increased to 230 °C at a heating rate of 20 °C·min<sup>-1</sup> and stabilized for 1 min. The temperatures of the injector and detector were 220 and 230 °C, respectively. The carrier gas was H<sub>2</sub> at a flow rate of 1.7 mL·min<sup>-1</sup>. Monosaccharides were identified by the retention time against the standards and quantified by comparing the areas of the sugar residues' peaks with the peak area of the internal standard.

**2.4.3.2. Methylation analysis.** The type of bond present in the polysaccharide was determined by methylation analysis as described in the literature [18]. The freeze-dried dialyzed EPS (2 mg) was dissolved in 1.0 mL of anhydrous dimethylsulfoxide and stirred for 2 h at room

temperature. After adding powdered NaOH pellets (40 mg) under argon atmosphere to the EPS solution and mixing for 30 min, samples underwent two steps of sequential methylation using CH<sub>3</sub>I (80 µL) for 20 min under magnetic agitation. Deionized water (2.0 mL) and dichloromethane (3.0 mL) were then added to the sample, and the dichloromethane phase was washed thrice with fresh deionized water (2.0 mL). The organic phase was evaporated to dryness and remethylated to obtain complete methylation of all free OH groups. Methylated samples were then hydrolyzed with 2.0 M trifluoroacetic acid at 121 °C for 1 h, cooled, and evaporated to dryness. Partially methylated sugars were reduced and acetylated as described before for neutral sugar content analysis. Partially methylated alditol acetates were separated and analyzed by gas chromatography–mass spectrometry (GC–MS) on a GC (6890 N Network, Agilent Technologies, Santa Clara, CA, USA) connected to an Agilent 5973 mass quadrupole selective detector operating in electron impact mode at 70 eV and scanning the *m/z* range of 50–700 in a 1 s cycle in a full scan mode acquisition. The GC was equipped with a capillary column (DB-1, J & W Scientific, Folsom, CA, USA) with 30 m length, 0.25 mm internal diameter and 0.10 µm film thickness. Prepared samples were then dissolved in anhydrous acetone (50 µL) and injected (0.2 µL) in split mode with the injector operating at 220 °C for 5 min. Helium was used as a carrier gas at a flow rate of 1.84 mL·min<sup>-1</sup> and a column head pressure of 124.1 kPa. The temperature program was as follows: the temperature was initially set at 80 °C, increased to 140 °C at a linear heating rate of 10 °C·min<sup>-1</sup>, and kept at this temperature for 5 min. Then it was increased to 150 °C at a heating rate of 0.5 °C·min<sup>-1</sup> and stabilized for 1 min. Finally, the temperature was increased to 250 °C at a heating rate of 15 °C·min<sup>-1</sup> and held at this value for a further 5 min. The sugar content of freeze-dried dialyzed EPS and the nature of glycosidic bonds were determined by comparing the characteristic retention times of standards injected separately under the same experimental conditions and further confirmed by comparing the MS fragmentation profiles with literature data.

### 2.4.4. Nuclear magnetic resonance spectroscopy

The chemical structure of freeze-dried dialyzed EPS was further assessed by <sup>1</sup>H NMR, <sup>13</sup>C NMR, <sup>1</sup>H–<sup>13</sup>C HSQC, and <sup>13</sup>C NMR DEPT 135 spectra obtained using a 400-MHz NMR spectrometer (Avance III, Bruker, Madison, WI, USA) equipped with a 5-mm inverse probe. The analysis was performed at 25 °C in D<sub>2</sub>O, applying the following acquisition parameters: 90° pulse, relaxation delay of 12 s and 200 scans. Chemical shifts of samples were expressed in ppm with respect to the internal standard of tetramethylsilane.

### 2.4.5. Electrospray ionization mass spectroscopy

The freeze-dried dialyzed EPS was evaluated by Electrospray Ionization Mass Spectroscopy (ESI-MS). Mass spectra were acquired in positive ionization mode using a quadrupole-time-of-flight electrospray ionization spectrometer (Compact, Bruker Daltonics, Billerica MA, USA) with a 45 V capillary voltage and a 200 °C source. An injection volume of 10 µL of a 2 mg·mL<sup>-1</sup> EPS aqueous solution diluted in 1:1 (v/v) water/methanol solution containing 0.1% (v/v) formic acid was used. The *m/z* range from 150 to 2000 was scanned, and the spectra were interpreted by the Bruker Daltonics Data Analysis software.

## 2.5. Determination of levan thermal properties

### 2.5.1. Thermogravimetric analysis

The onset decomposition temperature of freeze-dried dialyzed EPS was determined by Thermogravimetric Analysis (TGA) using a thermal mechanical analyzer (Setsys Evolution 1750, Setaram, Caluire, France). The sample (2.0 ± 0.2 mg) was heated in an alumina crucible, under nitrogen flow, over a temperature range from 20 to 1000 °C at a heating rate of 5 °C·min<sup>-1</sup>.

### 2.5.2. Differential scanning calorimetry

Temperatures and energy flows related to freeze-dried dialyzed EPS phase transitions were evaluated using a Differential Scanning Calorimeter (DSC) (Pyris Diamond DSC Autosampler, Perkin Elmer, Waltham, MA, USA) working at atmospheric pressure and previously calibrated with different standards with purity >99%. Temperature of samples ( $2.0 \pm 0.2$  mg) was increased from 20 to 100 °C at a linear heating rate of  $2\text{ °C}\cdot\text{min}^{-1}$  and stabilized for 1 min. Subsequently, the sample was cooled to 20 °C at a linear rate of  $50\text{ °C}\cdot\text{min}^{-1}$ , kept at this temperature for 3 min, and finally heated to 200 °C at a final linear rate of  $2\text{ °C}\cdot\text{min}^{-1}$ .

### 2.5.3. Dynamic mechanical analysis

The dynamic mechanical properties of freeze-dried dialyzed EPS were explored by Dynamic Mechanical Analysis (DMA). DMA curves of 10 mm long, 7.5 mm wide, and 0.60 mm thick rectangular-shaped samples were obtained using a Tritec 2000 DMA system (Triton Technologies, London, UK) operating in multiple tension mode (double strain) at 1/10 Hz with 0.020-mm displacement. The temperature was raised from  $-120$  to  $200$  °C at a constant heating rate of  $2\text{ °C}\cdot\text{min}^{-1}$ .

### 2.5.4. X-ray diffraction

Freeze-dried dialyzed EPS X-ray diffraction patterns were determined with a diffractometer (MiniFlex, Rigaku, Tokyo, Japan) under the following operating conditions: Cu K $\alpha$  radiation, 40 kV, 200 mA, scattering angles ( $2\theta$ ) of 5–50°. Scattering intensity data were recorded at a rate of  $0.5^\circ\cdot\text{min}^{-1}$  with a step resolution of  $0.02^\circ$ .

### 2.5.5. Scanning Electron Microscopy

Freeze-dried dialyzed EPS samples were gently placed on carbon conductive double-sided adhesive tapes fixed in a metal holder. Samples were coated with a very thin carbon layer by high-vacuum evaporation coating (Emitech K950X, France) and analyzed by Scanning Electron Microscopy using a Hitachi SU-70 microscope operating at 15 kV.

## 3. Results and discussion

### 3.1. Production of levan by *Paenibacillus* sp. #210 – upstream and downstream processing

The levan-producing bacterium was isolated from heavy crude oil samples obtained from a Brazilian oil field, identified as a strain of *Paenibacillus* and named *Paenibacillus* sp. #210 (Fig. S1). The growth curve on Mineral Salt Solution (MSS) supplemented with sucrose and ammonium nitrate (Fig. S2) in shake flask at the oil well temperature (40 °C) and 140 rpm showed that *Paenibacillus* sp. #210 had a very short lag phase (about 2 h), entered the exponential phase after 5 h and switched to the stationary phase after 11 h, reaching a maximum cell concentration of  $0.49\text{ g}\cdot\text{L}^{-1}$  that remained almost constant until the end of cultivation. The pH of the culture medium dropped from 7.0 to 5.9 due to acid production, as previously reported in studies on levan production by different strains of *Paenibacillus* sp. [19] and *Bacillus* sp. [20]. As shown by the  $pO_2$  curve, the isolate consumed all dissolved oxygen slightly before the beginning of the exponential phase, meaning that it initially grew aerobically but had the ability to subsequently grow in the absence of oxygen, consistent with its character of facultative anaerobic microorganism. The maximum specific growth rate ( $\mu_{\max}$ ) was  $0.45\text{ h}^{-1}$  corresponding to a doubling time of 1.52 h.

Although nutritionally restrictive, the use of enriched MSS ensured a satisfactory compromise between process time, EPS production and cell productivity. Levan production started only after a few hours and peaked ( $1.45\text{ g}\cdot\text{L}^{-1}$  of levan from just  $10\text{ g}\cdot\text{L}^{-1}$  sucrose) after reaching the stationary phase. It is well known from the literature that increasing the initial sucrose concentration in the medium leads to both increased growth of *Paenibacillus* strains and EPS production [19–21]. *Paenibacillus polymyxa* EJS-3 showed EPS production ranging from less than  $1\text{ g}\cdot\text{L}^{-1}$  to a maximum of  $22.82\text{ g}\cdot\text{L}^{-1}$  at a sucrose concentration of  $160\text{ g}\cdot\text{L}^{-1}$  [19].

Finally, the yields of biomass ( $Y_{X/S}$ ) and product (EPS) ( $Y_{P/S}$ ) on initial substrate were 0.045 and  $0.145\text{ g/g}$ , respectively.

Since downstream processing greatly influences the economic viability of any bioprocess, often being a dominant factor in the overall cost of products [22], a simple two-step purification process of the produced levan consisting of precipitation with ethanol followed by dialysis was applied. The main operations mentioned in the literature for the recovery of microbial levan from crude extract are ultrafiltration [20,23], ethanol precipitation [23,24], and chromatography [19,25]. The C, H, N and S contents determined by elemental analysis of a freeze-dried crude sample and a freeze-dried dialyzed sample (Table S1) suggest that the inorganic contaminants present in the crude sample, responsible for its relatively low carbon content, were effectively removed by the selected downstream protocol. The results obtained indicate that the partially purified sample was mainly composed of an organic fraction with a hydrogen/carbon molar ratio of 1.93, which provides a first indication of its glycosidic nature. Taking into consideration the hydrogen/carbon molar ratio of pure dehydrated hexose of 1.96, it is possible to estimate a glycosidic content of up to 98.5% for purified EPS, in line with the standard purity levels required for food additives. Furthermore, the efficacy of dialysis in purifying the product validates the use of membrane-based techniques (e.g., ultrafiltration) as cost-effective separation techniques for large-scale industrial production.

### 3.2. EPS physicochemical characterization

#### 3.2.1. Fourier transform infrared spectroscopy analysis

To confirm the glycosidic nature of the biocompound produced by *Paenibacillus* sp. #210, a preliminary characterization of the dialyzed freeze-dried sample was performed using Fourier Transform Infrared (FTIR) spectroscopy (Fig. 1).

The sample exhibited a complex peak pattern from  $3500$  to  $500\text{ cm}^{-1}$ , which is typical of the geometry and functional group configuration of carbohydrates [26]. The intense and rounded peak at around  $3500\text{--}3050\text{ cm}^{-1}$  was assigned to stretching vibrations of O–H groups, the two peaks at  $2941$  and  $2890\text{ cm}^{-1}$  to CH/CH $_2$  asymmetric and symmetric stretching vibrations modes, respectively [27], and the bands within the  $1500$  to  $1200\text{ cm}^{-1}$  region to CH deformation vibrational modes. The several sharp and sequential peaks between  $1200$  and  $800\text{ cm}^{-1}$  were assigned to the combination of OH bending ( $\delta\text{C—O—H}$ ), CO ( $\nu\text{C—O}$ ), CC ( $\nu\text{C—C}$ ) as well as C—O stretching and glycosidic bond, typically assumed as fingerprints of sugars in cyclic form [26,28]. The high degree of overlap of these absorption bands with those of fructose suggests that the biomolecule produced by *Paenibacillus* sp. #210 could be an EPS composed mainly of fructosyl units.

#### 3.2.2. Evaluation of monosaccharides composition and type of glycosidic bonds

To further characterize the produced EPS, the neutral sugar content of a dialyzed freeze-dried sample was determined. To ensure a complete hydrolysis of the biopolymer, the content of total sugar residues released during hydrolysis was determined under mild hydrolysis conditions ( $1.0\text{ M H}_2\text{SO}_4$  at  $70\text{ °C}$ ) and compared with that obtained under severe conditions ( $1.0\text{ M H}_2\text{SO}_4$  at  $100\text{ °C}$ ). Considering the total EPS mass and the previously mentioned purity degree, the results show that, under harsh hydrolysis conditions 75.0 and 55.6% of sugar residues were obtained (loss of about 25 and 50%) after 10 and 60 min, respectively, while after 150 min the loss was greater than 90% (Table S2).

Instead, under mild hydrolysis conditions, a maximum monosaccharide yield of 94.4% was observed after 30 min of hydrolysis, corresponding to the lowest sugar loss. This high yield of sugars confirms the high purity of the sample, as already indicated by other analytical techniques (i.e. FTIR and elemental analysis). As expected, even under mild conditions, the longer the hydrolysis time, the greater the degradation of monosaccharides (sugar loss of about 70.5% after 150 min).

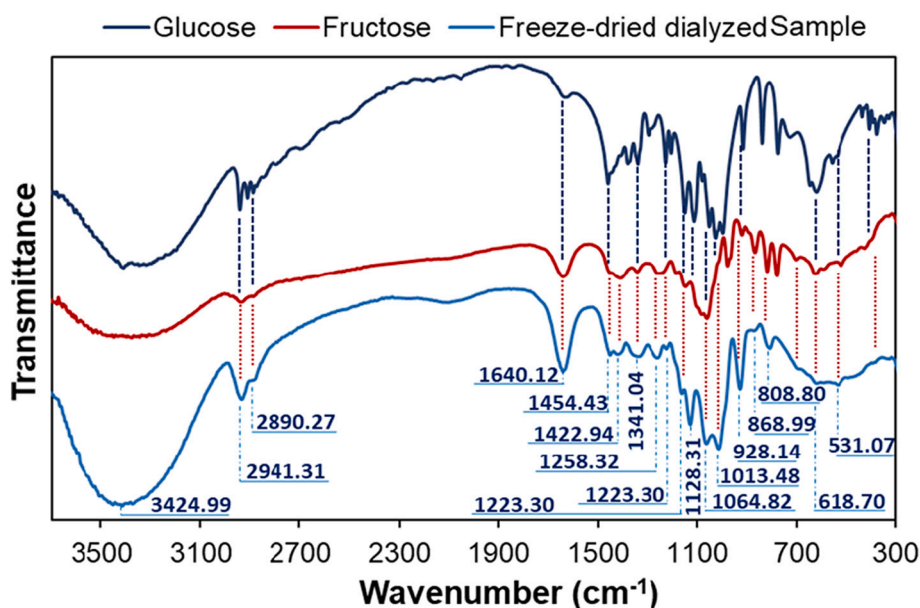


Fig. 1. FTIR spectra of glucose, fructose, and freeze-dried dialyzed sample of EPS produced by *Paenibacillus* sp. #210.

Therefore, the optimum hydrolysis conditions for the levan-type polymer are 70 °C for 30 min using 1 M sulfuric acid.

A monosaccharide composition of approximately 57% glucose and 43% mannose was determined (results not shown). During the sugar analysis procedure (reduction and acetylation), as fructose forms a new asymmetric center (chiral carbon) at C2 under reducing conditions, a racemic mixture of two diastereoisomers, namely mannitol (Man) and glucitol (Glc) [29], was obtained, with a slightly higher percentage of the latter. These results further support that the produced EPS is a homopolysaccharide with a fructose-based composition.

To shed light on the nature of FOS fructofuranosyl bonds, methylation analysis was carried out (Table 1). The obtained results show (Figs. S3–S7) that the main residues are 2,5,6-linked Glc (51.5%) and 2,5,6-linked Man (38.3%), confirming the presence of 2,6-linked Fru, the reduction of whose prochiral keto group actually led to the formation of Glc and Man alditols [29,30]. The presence of 2,5-linked Glc (2.9%) and 2,5-linked Man (2.2%) corresponded to terminally-linked fructose. Furthermore, the presence of 1,2,6-linked Glc and 1,2,6-linked Man (2.3%), attributed to 1,2,6-linked Fru, revealed that this polymer was even branched in position O1 to a small extent (4.6%), as reported in literature [8].

The relative ratio of each fructosyl unit was then calculated by summing the contributions of the respective mannitol and glucitol

**Table 1**  
Partially methylated alditol acetate derivatives of freeze-dried dialyzed FOS produced by *Paenibacillus* sp. #210.

Partially methylated alditol acetate	Relative proportion (%)	Type of bond
1,3,4,6-tetra-O-methyl(2,5-di-O-acetyl)-glucitol	2.85	D-Glcp-(2→
1,3,4,6-tetra-O-methyl(2,5-di-O-acetyl)-mannitol	2.22	D-Manp-(2→
1,3,4-tri-O-methyl(2,5,6-tri-O-acetyl)-glucitol	51.51	→6)-D-Glcp-(2→
1,3,4-tri-O-methyl(2,5,6-tri-O-acetyl)-mannitol	38.27	→6)-D-Manp-(2→
2,3,6-tri-O-methyl(1,4,5-tri-O-acetyl)-glucitol	0.53	→4)-D-Glcp-(1→
3,4-di-O-methyl(1,2,5,6-tetra-O-acetyl)-glucitol	2.34	→2,6)-D-Glcp-(1→
3,4-di-O-methyl(1,2,5,6-tetra-O-acetyl)-mannitol	2.29	→2,6)-D-Manp-(1→

derivatives, namely 5.0% terminal fructosyl units at C2 position, 89.7%  $\beta(2 \rightarrow 6)$  fructosyl units, 0.6% (1  $\rightarrow$  4) glucosyl units and 4.6%  $\beta(2 \rightarrow 1,2 \rightarrow 6)$  fructosyl branch point units. Thus, it was possible to infer that the FOS produced by *Paenibacillus* sp. #210 was mainly a linear polyfructan containing  $\beta(2 \rightarrow 6)$  bonds and  $\beta(2 \rightarrow 1)$  branching points, with a levan rather than an inulin structure. Additionally, the presence of 4-substituted glucose units suggests that the neokestose series of oligomers was also present in small amount. By calculating the ratio of  $\beta(2 \rightarrow 6)$  fructosyl residues by terminal and  $\beta(2 \rightarrow 1)$  fructosyl branching point units, it was possible to estimate an average degree of polymerization (DP) of approximately 18 and a ramification ratio of approximately 20.

### 3.2.3. Nuclear magnetic resonance spectroscopy

Fig. 2 shows the  $^1\text{H}$  Nuclear Magnetic Resonance (NMR) spectrum of dialyzed freeze-dried levan produced by *Paenibacillus* sp. #210, in the non-anomeric region ( $\delta$  3.5–4.30 ppm) of which seven signals can be seen, with chemical shifts corresponding to the hydrogen atoms of fructofuranosyl residues [12,31–33].

The signal observed in the anomeric region of  $^{13}\text{C}$  spectrum (Fig. 3) was assigned to the quaternary carbon atom ( $\delta$  107.06 ppm) involved in the oligomer intrachain linkage. Of the five resonance signals observed in the non-anomeric region, three were assigned to methine carbon atoms ( $\delta$  83.14, 79.20, 78.07 ppm) and two to those of methylene ( $\delta$  66.25, 62.82 ppm) [34]. The absence of  $^{13}\text{C}$  signals at the characteristic chemical shifts of glucose agrees with the results of sugar analysis, further validating the predominant presence of fructosyl residues in the biopolymer. Moreover, the absence of additional anomeric fructosyl signals of significant intensity in the  $^{13}\text{C}$  NMR and  $^{13}\text{C}$  distortionless-enhancement-by-polarization transfer (DEPT) spectra demonstrates that the FOS was mainly linear with a low level of branching, in agreement with the results of methylation analysis. All chemical shifts were consistent with those of oligo and polyfructans described in the literature [31–34]. The carbon chemical shift signals of isolated levans obtained from a wide variety of phylogenetically different bacteria (*Zymomonas mobilis*, [35], *Pseudomonas fluorescens* [36], *Chromohalobacter japonicus* BK-AB18 [37]) demonstrated high similarity.

To validate the  $^1\text{H}$  and  $^{13}\text{C}$  assignments, an additional analysis was performed using the 2D Heteronuclear Single-Quantum Correlation (HSQC) spectroscopy (Fig. 4). The analysis of the intra-residue cross-peak allowed to correlate the fructosyl hydrogens with their directly bonded carbon atoms ( $J_{\text{H/C}}$ ). The absence of any cross-peak for C2

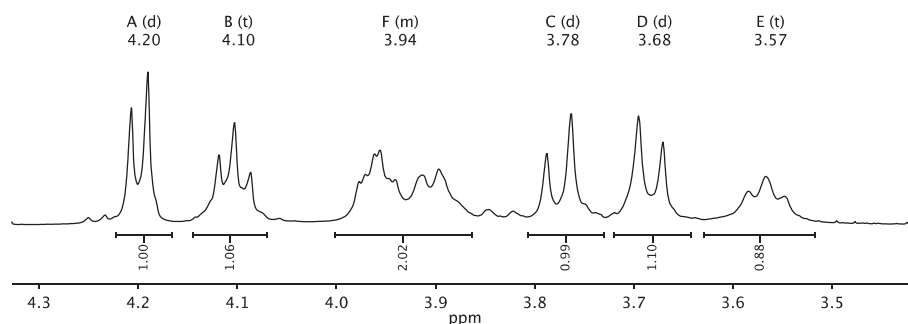


Fig. 2.  $^1\text{H}$  NMR spectrum of freeze-dried purified levan produced by *Paenibacillus* sp.#210.

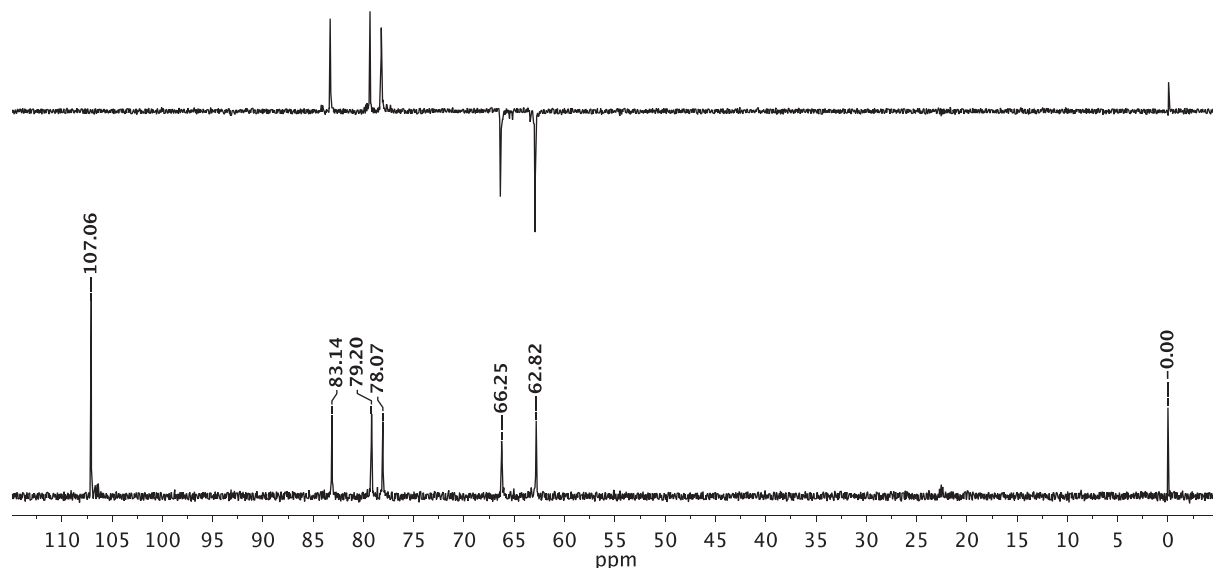


Fig. 3.  $^{13}\text{C}$  NMR and  $^{13}\text{C}$  DEPT 135 NMR spectra of freeze-dried purified levan produced by *Paenibacillus* sp.#210.

confirmed its quaternary anomeric character, typical of oligo and polyfructans configuration. Furthermore, cross-peaks between H1a-H1b/C1, H6a-H6b/C6, H5/C5, H4/C4 and H3/C3 are characteristic of levan type EPS [38]. Strong cross-peaks of long-range inter-residues ( $^3J_{\text{H/C}}$ ) between  $^1\text{H}$  and  $^{13}\text{C}$  were additionally detected by Heteronuclear Multiple-Bond Correlation spectroscopy (results not shown). The inter-residue correlations assigned between the non-anomeric H6 and the anomeric C2 signals confirmed the  $[\rightarrow 6)\text{-}\beta\text{-D-Fruf-(2}\rightarrow)]_n$ -based structure previously suggested by methylation analysis [12,34]. The signals from the  $^1\text{H}$ ,  $^{13}\text{C}$  NMR, and HSQC spectra refer to the characteristic  $\beta$ -(2,6) linkages of fructose residues similar to those detected by NMR/FTIP for the extracellular levan produced by *Bacillus siamensis* NR 11274.1 [39].

### 3.2.4. Electrospray ionization mass spectroscopy

Levan composition was further investigated in terms of DP of the oligomers by Electrospray Ionization Mass Spectroscopy (ESI-MS) (Fig. S8). Levan average DP was calculated for mono-charged sodium adducts of anhydrous terminal fructose, considering the loss of one water molecule per glycosidic bond, by the equation  $m/z = [\text{hexose } M_w (180) \times \text{DP}] - [\text{H}_2\text{O } M_w (18) \times \text{DP}] + \text{Na } A_w (23)$  [40].

By the analysis of  $m/z$  peaks, mono-charged sodium adducts of levan oligomers with DP in the range 2–11 were identified, namely  $F_2$  ( $m/z = 372.1$ ),  $F_3$  ( $m/z = 509.2$ ),  $F_4$  ( $m/z = 671.3$ ),  $F_5$  ( $m/z = 833.4$ ),  $F_6$  ( $m/z = 995.5$ ),  $F_7$  ( $m/z = 1157.5$ ),  $F_8$  ( $m/z = 1319.7$ ),  $F_9$  ( $m/z = 1481.6$ ),  $F_{10}$  ( $m/z = 1643.6$ ) and  $F_{11}$  ( $m/z = 1805.5$ ). Since such a distribution was far below the one previously highlighted by the methylation analysis,

the presence of high molecular weight chains was also checked considering the existence of multiply charged adducts. As for an average levan DP of 18 ( $M_w = 2918,88 \text{ g}\cdot\text{mol}^{-1}$ ), a molecular adduct with charge equal to six ( $z = 6$ ), i.e. having six  $\text{Na}^+$  and a corresponding molecular ion with  $m/z = 509.2$ , was considered to be present in the levan blend. Although the determined molecular weight was less than the cut-off size used for dialysis, retention of the biopolymer by the membrane was successful, as evidenced by the whitish to blue color of the solution, as a likely result of biopolymer aggregation and nano-micro particles formation. It has been reported that such an aggregation can result from levan self-assembly in water into micellar aggregates of larger molecular weight (up to 2200 kDa) when the critical aggregation concentration threshold is reached ( $0.05 \text{ mg}\cdot\text{mL}^{-1}$  for levan-type FOS from microbial sources) [41]. Considering other levans produced by *Paenibacillus* sp., they generally have a high molecular weight, even higher than that determined in this study. For instance, Han and Clarke [20] reported a molecular weight of up to  $2 \times 10^6$  Da for the levan produced by *Paenibacillus polymyxa* NRRL B-18475 grown on sucrose, and Liu et al. [19] characterized two EPS from *Paenibacillus polymyxa* EJS-3 with molecular weights of  $1.22 \times 10^6$  and  $8.69 \times 10^5$  Da, respectively. Polyfructans with DP > 11 were also considered to be present at pre-assigned  $m/z$  peaks under the same multiple charge phenomenon, namely  $F_{14}$  ( $m/z = 1157.5$ ;  $z = 2$ ) and  $F_{15}$  ( $m/z = 833$ ;  $z = 3$ ). Similar multiple charge occurrence was reported for partially acid-hydrolyzed manuronans and confirmed by the analysis of molecular ion fragmentation profiles [42].

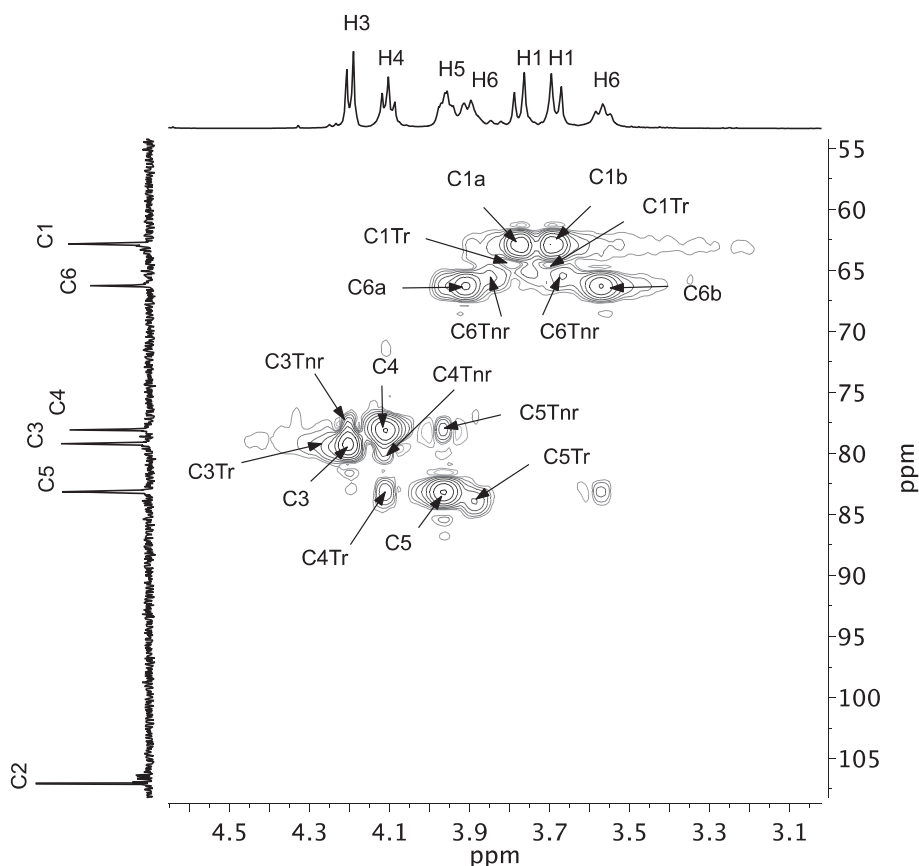


Fig. 4. HSQC spectrum of crude exopolysaccharide produced by *Paenibacillus* sp. #210.

### 3.2.5. X-ray diffraction

The X-ray diffractogram of the produced levan (Fig. S9) showed a broad halo pattern with a single peak at  $18^\circ$  ( $2\theta$ ), pointing out an amorphous structure similar to that reported elsewhere [43,44]. The amorphous nature of a biomolecule is a strong indication not only of its likely low ability to develop a crystalline structure but also of possible protective and stabilizing properties in medical and pharmaceutical applications. However, although little information is available on levan crystallization mechanisms, some papers have reported the detection of different diffraction peaks related to semi-crystalline domains in high molecular weight levans produced by different microorganisms [28,45].

### 3.3. Scanning electron microscopy

Fig. 5 shows the microstructure and surface morphology of freeze-dried *Paenibacillus* sp. #210 levan particles detected by Scanning Electron Microscopy (SEM). Three main morphologies can be observed, namely ellipsoidal or spheroidal amorphous particles with variable average size, entangled filament networks, and uniform, smooth, apparently thin and malleable films. According to the literature, bacterial levans in aqueous solution often assume a compact morphology with spherical symmetry [46].

Such a morphological diversity may have been the result of different transformations of levan particles that occurred during freezing and lyophilization process. Regardless of the phenomena underlying such physical transformations, i.e., aggregation, adsorption, fusion, deformation and/or elongation, it is evident the high versatility of *Paenibacillus* sp. #210 levan to form a series of different microscopic structures. These observations support its potential use in a large number of different applications, including the preparation of nanoparticles [41], microparticles for drug delivery [47], fibers [44] and/or films [48].

### 3.4. Thermal analysis

#### 3.4.1. Thermogravimetric analysis

Considering the potential applicability of levans mainly in the food and polymer sectors, their thermal features are of great importance. Therefore, the thermal stability of *Paenibacillus* sp. #210 levan was assessed following its decomposition profile by thermogravimetric analysis (TGA) and derivative thermogravimetry (DTG). Fig. 6 shows the experimental results in terms of weight loss and derivative weight loss curves as functions of temperature.

It can be seen that the levan underwent an initial weight loss of approximately 9% between 20 and  $100^\circ\text{C}$  due to moisture evaporation [45], while no significant loss was observed in the temperature range  $100$ – $200^\circ\text{C}$ . A second fast weight loss event occurred at  $200$ – $250^\circ\text{C}$  and another at  $250$ – $400^\circ\text{C}$ , accounting for 30 and 31% of total weight loss, respectively. A further increase in temperature up to  $1000^\circ\text{C}$  resulted in a gradual weight loss of only 10%, corresponding to a total levan degradation of 81%. Such weight losses suggest, after moisture release, sequential break of  $\beta(2 \rightarrow 1)$  branch point linkages,  $\beta(2 \rightarrow 6)$  linkages, and furanose rings along with other char-forming reactions [49]. DTG pointed to a degradation temperature ( $T_d$ ) of  $218^\circ\text{C}$ , which would allow the use of levan to synthesize different products using processing technologies at remarkably high temperatures [50]. Both levan  $T_d$  and weight loss profile are in agreement with those reported in the literature for similar microbial levans [51–53].

#### 3.4.2. Differential scanning calorimetry

Fig. 7 shows the levan thermal phase behavior obtained by Differential Scanning Calorimetry (DSC) with a sequential heat-cool-reheat profile.

According to these results, *Paenibacillus* sp. #210 levan exhibited an endothermic (heating cycle) and an exothermic (cooling cycle)

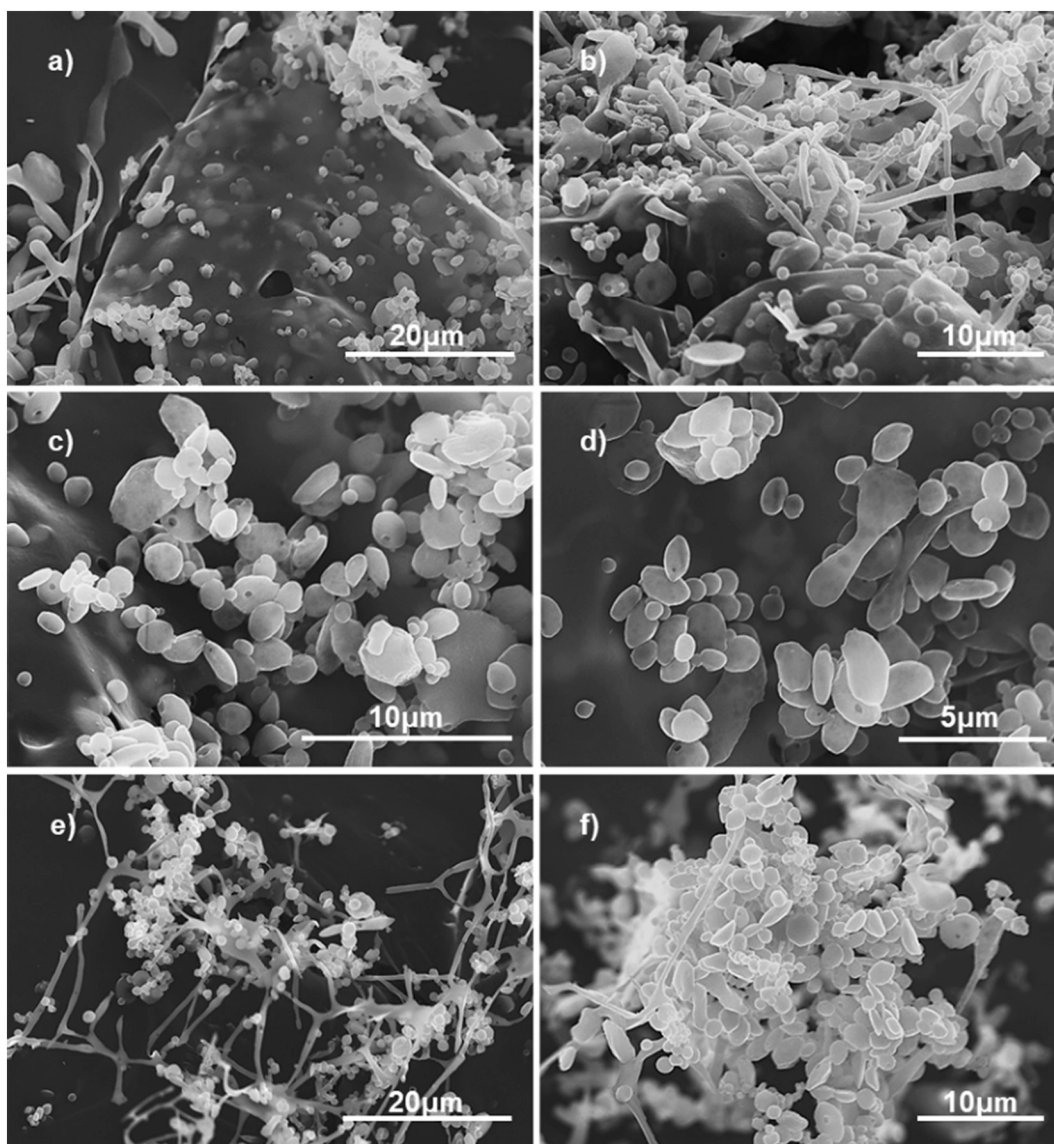


Fig. 5. Microstructure and surface morphology of *Paenibacillus* sp. #210 freeze-dried levan observed by SEM.

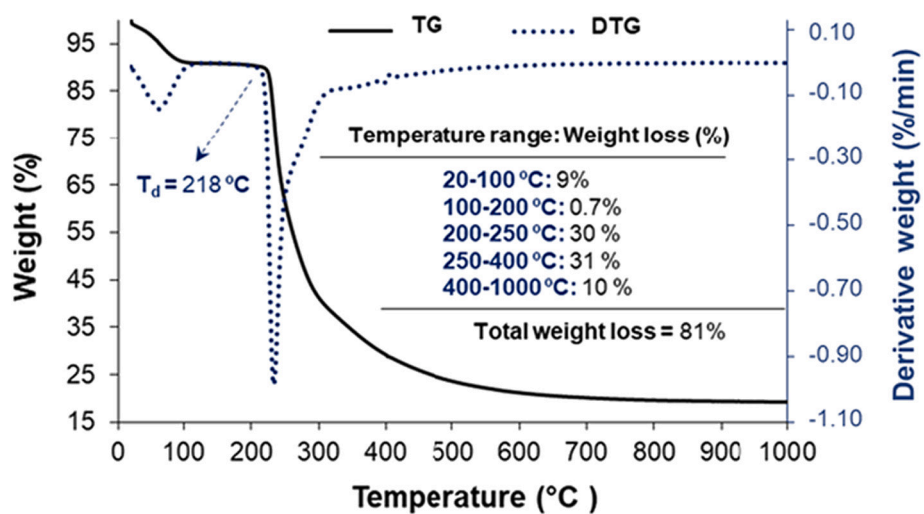


Fig. 6. Results of thermogravimetric analysis (TGA) and derivative thermogravimetry (DTG) of *Paenibacillus* sp. #210 levan.



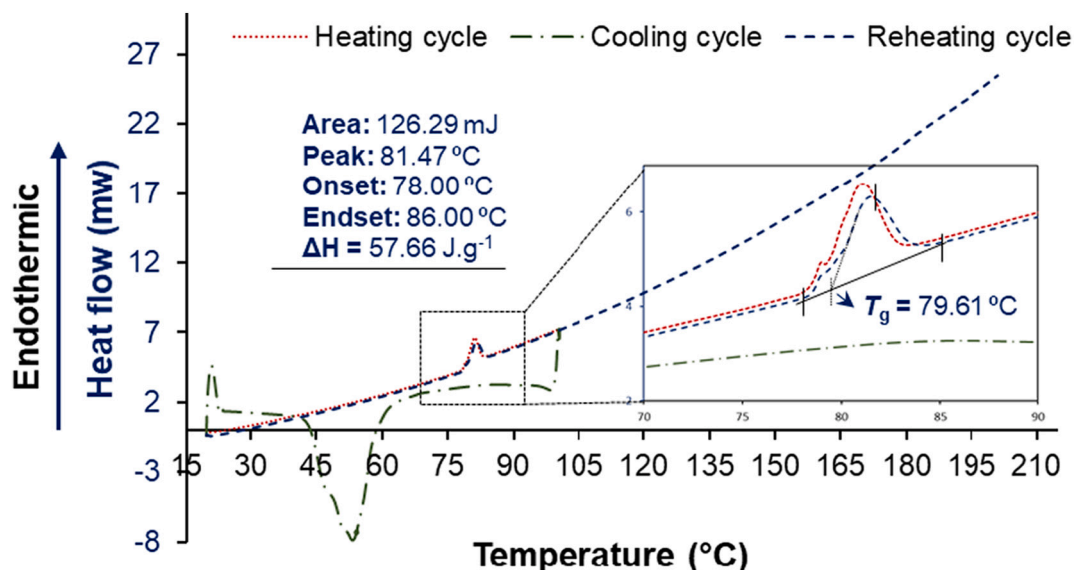


Fig. 7. DSC thermogram of *Paenibacillus* sp. #210 freeze-dried dialyzed levan considering an initial heating cycle up to 100 °C, followed by a cooling cycle to 20 °C and a final reheating cycle to 200 °C.

transition event with onset temperatures of 78 and 65 °C, and endset temperatures of 86 and 40 °C, respectively. Since the endothermic transition event was reversible in both heating cycles, any relationship with water evaporation was excluded. Taking into consideration the amorphous structure of levan highlighted earlier by the X-ray diffraction analysis, the observed phase transition can be related to a glass transition, *i.e.*, a transition of the amorphous polymer from a glassy-hard to a soft state when heated [54]. Even though reproducible, the reheating endothermic peak showed a maximum temperature deviation of 81.10 to 81.47 °C. This occurrence can be ascribed to the increased segmental molecular motion and biopolymer internal friction after sample moisture loss during the first heating cycle [55,56], due to several reorganizations of polymer water holding sites and the creation of new polymer-polymer intermolecular interactions [54]. These considerations agree with the observation of a reduction in FOS glass transition temperature ( $T_g$ ) as the water content increased [57].

The intersection of the baseline tangent with that of the endothermic transition peak with the highest slope made it possible to estimate a levan  $T_g$  of 79.61 °C, corresponding to an enthalpy change of 57.66 J.g<sup>-1</sup> [54]. Such a  $T_g$  is close to that (75.5 °C) reported for a *Bacillus* sp. levan [28], but much lower than those of other levans produced by a different *Bacillus* strain (140 °C) [50] and by *Halomonas smyrnensis* AAD6<sup>T</sup> (150 °C) [47]. Since no other *exo*-endothermic event of thermal degradation was detected after the assigned  $T_g$  event, it was possible to infer that *Paenibacillus* sp. #210 levan was thermally stable in the tested temperature range, thus confirming the thermal stability results obtained from the TGA.

### 3.5. Dynamic mechanical analysis

Considering that structural changes in polymers affect mechanical properties at a proportionally higher level than their specific heat [58], a final study on levan thermomechanical properties was conducted using the Dynamic Mechanical Analysis (DMA).

Fig. 8 shows the temperature dependence of storage modulus ( $G'$ ), loss modulus ( $G''$ ) and damping coefficient ( $\tan \delta = G''/G'$ ). It can be seen that levan underwent a series of changes in its mechanical properties due to the temperature increase, which included, in addition to the previously described glass transition detected by DSC, transitions events associated with small molecular motions occurring in the glassy or rubbery state region. As the material was heated in the glassy state

region, in which the molecules are tightly compacted, the  $G'$  curve that expresses the biopolymer elastic behavior progressively decreased, while  $G''$  and  $\tan \delta$  curves, which measure its viscous response and energy dissipation, respectively, gradually increased. Levan expanded progressively, with an increase in the free volume of its chain segments, until reaching the so-called gamma transition ( $T_\gamma$ ), in which both local main-chain groups and intramolecular chain segments, made up of four to six atoms, began to move. [59]. A further rise in temperature also resulted in an increase in the  $G''$  and  $\tan \delta$  curves, which suggests that the side chains and localized levan groups gained enough space to move, evolving into a structural transition classified as beta transition ( $T_\beta$ ) and belonging to the so-called transition region.

Due to this transition, it is likely that levan side groups began to move based on cooperative movements from the main chain, acquiring a higher toughness profile. By continuing to heat the sample, the amorphous levan chains exhibited coordinated long-chain extensive segmental motions within polymer segments of the main chain, and  $T_g$ , also called alpha transition ( $T_\alpha$ ), was achieved. At this point, levan lost its glass-like rigid properties and gradually took on a more rubbery and flexible state [54]. Since a totally amorphous polymer has no melting point by definition, heating the levan beyond its  $T_g$  may have caused it to assume a softened nature up to a final viscous state, until its degradation temperature was reached.

Since that, contrarily to the melting peak,  $T_g$ , as well as other transitions like  $T_\beta$  and  $T_\gamma$ , is frequency-dependent, its assignment was validated by comparing the 1 and 10 Hz  $\tan \delta$  curves, and it was calculated using the 1 Hz  $\tan \delta$  as a reference (zoomed-in section of Fig. 8c). Based on the obtained results, three clear frequency-dependent transition peaks were detected beyond the  $T_g$  temperature measured by DSC. A first transition event was detected at onset of 75.5 °C, endset of 103.3 °C and maximum  $\tan \delta$  of 86.60 °C. Such a temperature differed from that obtained by DSC by only 7 °C, *i.e.*, a difference lower than that usually reported in the literature (10–20 °C), which suggests that the observed thermomechanical profile was related to the endothermic event detected by DSC. A second transition event was detected at onset of 155.7 °C, endset of 179.2 °C and maximum  $\tan \delta$  of 170.9 °C, corresponding approximately to a 69 °C difference compared to the first transition peak, and a third one at onset of 179.2 °C, endset of 195.5 °C and maximum  $\tan \delta$  of 185.2 °C, corresponding approximately to 109 and 24 °C differences compared to the first and second transition peaks, respectively. These results provided shreds of evidence for the existence

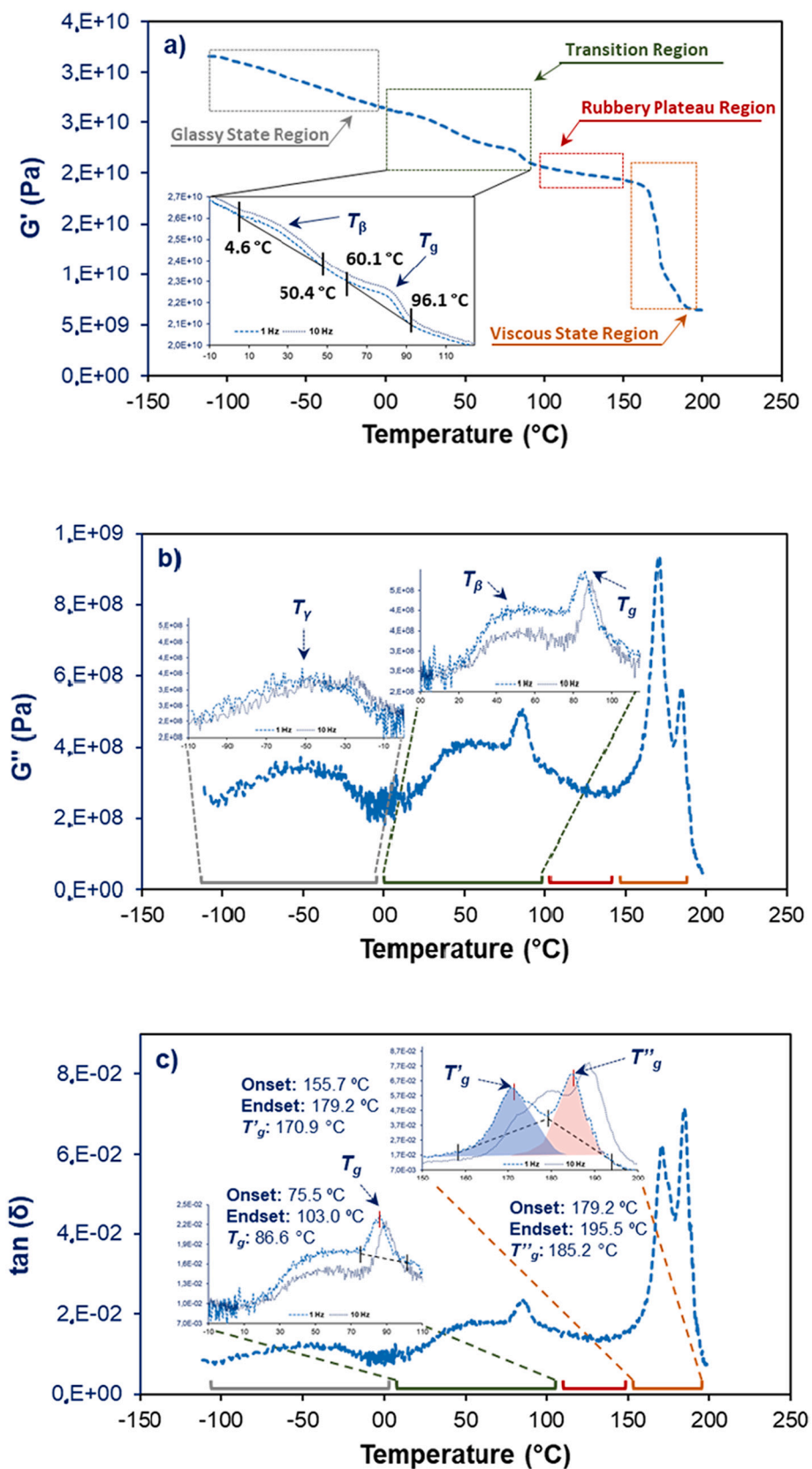


Fig. 8. DMA plots of *Paemibacillus* sp. #210 freeze-dried dialyzed levan (a) storage modulus ( $G'$ ), (b) loss modulus ( $G''$ ) and (c)  $\tan \delta$  as functions of temperature.

of three different  $T_g$  resulting from the mixture of oligo and polyfructans having significantly distinct DP (small, medium, and high DP). The fact that DSC analysis did not detect below 200 °C any enthalpy event highlighting the two additional  $T_g$  temperatures is justified by its lower sensitivity compared to DMA [60]. Although the DSC and TGA results did not provide any evidence of thermal decomposition below 200 °C, strong insights support the high susceptibility of low-DP levan oligomers to undergo structural deformation after mechanical stress application, especially at high temperatures [61]. This consideration is justified by significantly high differences in  $T_g$  temperatures and viscoelastic profiles of levan mixtures with different DP values, especially between low-medium and medium-high DP [61,62]. As it is possible to observe, levan mixture stiffness and damping behavior decreased after each  $T_g$  transition, mainly at temperatures >150 °C. In this temperature range, levan may have been more susceptible to deformations in its structure as a likely result of a reduced ability of the oligomers to disperse mechanical energy through internal molecular movements.

These results taken together suggest a temperature range of 25–150 °C as the optimum one for thermomechanical processing of levan mixture [50]. However, further studies are required to fully understand the events occurring in complex mixtures of oligo and polyfructans.

The thermostability of levan and its noteworthy mechanical properties would enable the fabrication of composite scaffolds by blending this biocompatible polymer with hydroxyapatite or sintered hydroxyapatite, which could be exploited as bone graft substitutes for bone tissue engineering [63].

#### 4. Conclusions

A polydisperse levan-type EPS composed of oligomers with a variable DP was successfully produced at a concentration of 1.45 g·L<sup>-1</sup> using a *Paenibacillus* strain isolated from Brazilian crude oil. The isolated strain was grown in shake flasks at 40 °C (oil field temperature), using a mineral salt solution supplemented with sucrose (10.0 g·L<sup>-1</sup>) and ammonium nitrate (2.0 g·L<sup>-1</sup>) as carbon and nitrogen sources, respectively, obtaining an EPS yield on initial substrate of 0.145 g/g. After purification, an estimated purity percentage of up to 98 wt% was achieved. The EPS was characterized as a mainly linear levan, with averages degrees of polymerization and branching of approximately 18 and 20, respectively. A degradation temperature of 218 °C and a glass transition temperature of 79.61 °C were determined by TGA and DSC. Based on thermomechanical data, an estimated optimum processing temperature has been defined between 25 and 150 °C, which supports its use for the synthesis of different products with different processing technologies even at high temperatures. Levan morphological features and amorphous nature highlight its potential not only in the food, biopharmaceutical, and nutraceutical sectors, but also in emerging applications in materials' science. To significantly increase the process yield, new efforts should be made to optimize levan production in the near future. Nevertheless, the physicochemical characteristics of these sugar-based products are crucial to fully validate their technological potential. The next effort will deal with the use of this EPS in food applications.

#### CRedit authorship contribution statement

CMNM: conceptualization, methodology, investigation, formal analysis, visualization, writing – original draft, review & editing. RCO: investigation, methodology. RKBF: investigation, methodology. ACPM: investigation, methodology. WAP: investigation, methodology. EJG: investigation, methodology. DVE: formal analysis, review & editing. AC: review & editing. JHPMS: review & editing. CN: review & editing. LRR and RPSO: conceptualization, supervision, project administration, funding acquisition, methodology, writing - review & editing. All authors read and approved the final manuscript.

#### Declaration of competing interest

There are no competing financial interests or personal relationships to declare.

#### Acknowledgements

The authors are grateful to the financial support by São Paulo Research Foundation (FAPESP) within Grants 2020/13271-6 and 2018/25511-1. Additionally, the authors acknowledge the financial support by National Council for Scientific and Technological Development – CNPq and by Coordination for the Improvement of Higher Education Personnel (CAPES), Finance Code 001. In addition, this study was supported by the Portuguese Science Foundation (FCT) under the scope of the strategic funding of UID/BIO/04469/2020 unit and the Project FOSYNBIO (POCI-01-0145-FEDER-029549).

#### Appendix A. Supplementary data

Supplementary data to this article can be found online at <https://doi.org/10.1016/j.ijbiomac.2021.07.036>.

#### References

- [1] M. Sabater-Molina, E. Larqué, F. Torrella, S. Zamora, Dietary fructooligosaccharides and potential benefits on health, *J. Physiol. Biochem.* 65 (2009) 315–328, <https://doi.org/10.1007/BF03180584>.
- [2] B.C. Tunland Fructooligosaccharides and other fructans: structures and occurrence, production, regulatory aspects, food applications, and nutritional health significance Oligosaccharides in Food and Agriculture, ACS Symposium Series, Washington 849 10.1021/bk-2003-0849.ch011.
- [3] C. Amorim, S.C. Silvério, B.B. Cardoso, J.J. Alves, M.A. Pereira, L.R. Rodrigues, In vitro fermentation of raffinose to unravel its potential as prebiotic ingredient, *LWT Food Sci. Technol.* 126 (2020), 109322, <https://doi.org/10.1016/j.lwt.2020.109322>.
- [4] Y. Guigoz, F. Rochat, G. Perruisseau-Carrier, I. Rochat, E.J. Schiffrin, Effects of oligosaccharide on the faecal flora and non-specific immune system in elderly people, *Nutr. Res.* 22 (2002) 13–25, [https://doi.org/10.1016/S0271-5317\(01\)00354-2](https://doi.org/10.1016/S0271-5317(01)00354-2).
- [5] F. Capitán-Cañadas, B. Ocón, C.J. Aranda, A. Anzola, M.D. Suárez, A. Zarzuelo, F. S. de Medina, O. Martínez-Augustín, Fructooligosaccharides exert intestinal anti-inflammatory activity in the CD4+ CD62L+ T cell transfer model of colitis in C57BL/6J mice, *Eur. J. Nutr.* 55 (2016) 1445–1454, <https://doi.org/10.1007/s00394-015-0962-6>.
- [6] F. Lara-Villoslada, O. De Haro, D. Camuesco, M. Comalada, J. Velasco, A. Zarzuelo, J. Xaus, J. Galvez, Short-chain fructooligosaccharides, in spite of being fermented in the upper part of the large intestine, have anti-inflammatory activity in the TNBS model of colitis, *Eur. J. Nutr.* 45 (2006) 418–425, <https://doi.org/10.1007/s00394-006-0610-2>.
- [7] M.J. Mabel, P.T. Sangeetha, K. Platel, K. Srinivasan, S.G. Prapulla, Physicochemical characterization of fructooligosaccharides and evaluation of their suitability as a potential sweetener for diabetics, *Carbohydr. Res.* 343 (2008) 56–66, <https://doi.org/10.1016/j.carres.2007.10.012>.
- [8] C. Hundscheil, A. Braun, D. Wefers, R. Vogel, F. Jakob, Size-dependent variability in flow and viscoelastic behavior of Levan produced by gluconobacter albidus TMW 2.1191, *Foods* 9 (2020) 192, <https://doi.org/10.3390/foods9020192>.
- [9] P.B. Smith, Safety of short-chain fructooligosaccharides and GRAS affirmation by the U.S. FDA, in: *Bioscience and Microflora* 21, 2002, pp. 27–29, <https://doi.org/10.12938/bifidus1996.21.27>.
- [10] Agency Response Letter GRAS Notice No. GRN 000605, FDA, 2006. <https://www.fda.gov/food/gras-notice-inventory/agency-response-letter-gras-notice-no-grn-000605>. (Accessed 4 November 2020).
- [11] C.G. Kumar, S. Sripada, Y. Poornachandra, Status and future prospects of fructooligosaccharides as nutraceuticals, in: *Role of Materials Science in Food Bioengineering*, Elsevier, 2018, pp. 451–503, <https://doi.org/10.1016/B978-0-12-811448-3.00014-0>.
- [12] R. Srikanth, C.H.S.S.S. Reddy, G. Siddhartha, M.J. Ramaiah, K.B. Uppuluri, Review on production, characterization and applications of microbial Levan, *Carbohydr. Polym.* 120 (2015) 102–114, <https://doi.org/10.1016/j.carbpol.2014.12.003>.
- [13] N. Benkeblia, Fructooligosaccharides and fructans analysis in plants and food crops, *J. Chromatogr. A* 1313 (2013) 54–61, <https://doi.org/10.1016/j.chroma.2013.08.013>.
- [14] F. Freitas, C.A.V. Torres, M.A.M. Reis, Engineering aspects of microbial exopolysaccharide production, *Bioresour. Technol.* 245 (2017) 1674–1683, <https://doi.org/10.1016/j.biortech.2017.05.092>.
- [15] A.L. Dominguez, L.R. Rodrigues, N.M. Lima, J.A. Teixeira, An overview of the recent developments on fructooligosaccharide production and applications, *Food Bioprocess Technol.* 7 (2014) 324–337, <https://doi.org/10.1007/s11947-013-1221-6>.

- [16] E.J. Guđiņa, J.F.B. Pereira, R. Costa, J.A.P. Coutinho, J.A. Teixeira, L.R. Rodrigues, Biosurfactant-producing and oil-degrading *Bacillus subtilis* strains enhance oil recovery in laboratory sand-pack columns, *J. Hazard. Mater.* 261 (2013) 106–113, <https://doi.org/10.1016/j.jhazmat.2013.06.071>.
- [17] A.S. Silva, C. Nunes, M.A. Coimbra, L.F. Guido, Composition of pectic polysaccharides in a portuguese apple (*Malus domestica* borkh. cv bravo de Esmolfe), *Sci. Agric.* 71 (2014) 331–336, <https://doi.org/10.1590/0103-9016-2013-0333>.
- [18] C.O. Pandeirada, É. Maricato, S.S. Ferreira, V.G. Correia, B.A. Pinheiro, D. V. Evtuguin, A.S. Palma, A. Correia, M. Vilanova, M.A. Coimbra, C. Nunes, Structural analysis and potential immunostimulatory activity of nannochloropsis oculata polysaccharides, *Carbohydr. Polym.* 222 (2019), 114962, <https://doi.org/10.1016/j.carbpol.2019.06.001>.
- [19] J. Liu, J. Luo, H. Ye, Y. Sun, Z. Lu, X. Zeng, Production, characterization and antioxidant activities in vitro of exopolysaccharides from endophytic bacterium *paenibacillus polymyxa* EJS-3, *Carbohydr. Polym.* 78 (2009) 275–281, <https://doi.org/10.1016/j.carbpol.2009.03.046>.
- [20] Y.W. Han, M.A. Clarke, Production and characterization of microbial Levan, *J. Agric. Food Chem.* 38 (1990) 393–396, <https://doi.org/10.1021/jf00092a011>.
- [21] I.Y. Lee, W.T. Seo, G.J. Kim, M.K. Kim, S.G. Ahn, G.S. Kwon, Y.H. Park, Optimization of fermentation conditions for production of exopolysaccharide by *bacillus polymyxa*, *Bioprocess Eng.* 16 (1997) 71–75, <https://doi.org/10.1007/s004490050290>.
- [22] B. Atkinson, P. Sainter, Development of downstream processing, *J. Chem. Technol. Biotechnol.* 32 (2007) 100–108, <https://doi.org/10.1002/jctb.5030320114>.
- [23] W. Zhang, X. Zhang, L. Cai, R. Chen, Q. Zhang, X. Wang, Determination of Levan from *Bacillus licheniformis* by ultraviolet spectrophotometry, *Trop. J. Pharm. Res.* 14 (2015) 679–685, <https://doi.org/10.4314/tjpr.v14i4.17>.
- [24] F.C.B.C. de Melo, C.T.B.V. Zaia, M.A.P.C. Celligoi, Levan from *Bacillus subtilis* natto: its effects in normal and in streptozotocin-diabetic rats, *Braz. J. Microbiol.* 43 (2012) 1613–1619, <https://doi.org/10.1590/S1517-83822012000400046>.
- [25] D. Qiao, B. Hu, D. Gan, Y. Sun, H. Ye, X. Zeng, Extraction optimized by using response surface methodology, purification and preliminary characterization of polysaccharides from *Hyriopsis cumingii*, *Carbohydr. Polym.* 76 (2009) 422–429, <https://doi.org/10.1016/j.carbpol.2008.11.004>.
- [26] M. Kacuráková, M. Mathlouthi, FTIR and laser-raman spectra of oligosaccharides in water: characterization of the glycosidic bond, *Carbohydr. Res.* 284 (1996) 145–157, [https://doi.org/10.1016/0008-6215\(95\)00412-2](https://doi.org/10.1016/0008-6215(95)00412-2).
- [27] W.F. Wolkers, A.E. Oliver, F. Tablin, J.H. Crowe, A fourier-transform infrared spectroscopy study of sugar glasses, *Carbohydr. Res.* 339 (2004) 1077–1085, <https://doi.org/10.1016/j.carres.2004.01.016>.
- [28] X. Chen, H. Gao, H.J. Ploehn, Montmorillonite-Levan nanocomposites with improved thermal and mechanical properties, *Carbohydr. Polym.* 101 (2014) 565–573, <https://doi.org/10.1016/j.carbpol.2013.09.073>.
- [29] McGinnis, Biermann, *Analysis of Carbohydrates by GLC and MS*, CRC Press, Florida, 1988.
- [30] M. Kambourova, E.T. Oner, A. Poli, Exopolysaccharides from prokaryotic microorganisms-promising sources for white biotechnology processes, in: *Industrial Biorefineries and White Biotechnology*, Elsevier, 2015, pp. 523–554.
- [31] S. Cérantola, N. Kervarec, R. Pichon, C. Magné, M.A. Bessieres, E. Deslandes, NMR characterisation of inulin-type fructooligosaccharides as the major water-soluble carbohydrates from *Matricaria maritima* (L.), *Carbohydr. Res.* 339 (2004) 2445–2449, <https://doi.org/10.1016/j.carres.2004.07.020>.
- [32] A.J.B. De Oliveira, R.A.C. Gonçalves, T.P.C. Chierrito, M.M. Dos Santos, L.M. De Souza, P.A.J. Gorin, G.L. Sasaki, M. Iacomini, Structure and degree of polymerisation of fructooligosaccharides present in roots and leaves of *Stevia rebaudiana* (Bert.) bertonii, *Food Chem.* 129 (2011) 305–311, <https://doi.org/10.1016/j.foodchem.2011.04.057>.
- [33] M. Wack, W. Blaschek, Determination of the structure and degree of polymerisation of fructans from *Echinacea purpurea* roots, *Carbohydr. Res.* 341 (2006) 1147–1153, <https://doi.org/10.1016/j.carres.2006.03.034>.
- [34] C. Matsuzaki, C. Takagaki, Y. Tomabechi, L.S. Forsberg, C. Heiss, P. Azadi, K. Matsumoto, T. Katoh, K. Hosomi, J. Kunisawa, K. Yamamoto, K. Hisa, Structural characterization of the immunostimulatory exopolysaccharide produced by *leuconostoc mesenteroides* strain NTM048, *Carbohydr. Res.* 448 (2017) 95–102, <https://doi.org/10.1016/j.carres.2017.06.004>.
- [35] J.W. Kwak, Y.G. Seo, K.B. Song, S.K. Rhee, An enzyme-linked immunoassay for the levansucrase of *zymomonas mobilis* using specific antibodies produced against the cloned enzyme, *Biotechnol. Tech.* 10 (1996) 127–132, <https://doi.org/10.1007/BF00765195>.
- [36] N.R. Jathore, M.v. Bule, A.v. Tilay, U.S. Annature, Microbial levan from *Pseudomonas fluorescens*: characterization and medium optimization for enhanced production, *Food Sci. Biotechnol.* 21 (2012) 1045–1053, <https://doi.org/10.1007/s10068-012-0136-8>.
- [37] D.Q. Nasir, D. Wahyuningrum, R. Hertadi, Screening and characterization of Levan secreted by halophilic bacterium of *halomonas* and *chromohalobacter* genes originated from bledug kuuwu mud crater, *Procedia Chemistry.* 16 (2015) 272–278, <https://doi.org/10.1016/j.proche.2015.12.050>.
- [38] E.O. Joaquim, A.H. Hayashi, L.M.B. Torres, R.C.L. Figueiredo-Ribeiro, N. Shiomi, F. S. de Sousa, J.H.G. Lago, M.A.M. Carvalho, Chemical structure and localization of Levan, the predominant fructan type in underground systems of *Gomphrena marginata* (amaranthaceae), *Front. Plant Sci.* 9 (2018) 1745, <https://doi.org/10.3389/fpls.2018.01745>.
- [39] N. Thakham, S. Thaweesak, N. Teerakulkittipong, N. Traiosot, A. Kaikaw, G. A. Lirio, W. Jangiam, Structural characterization of functional ingredient Levan synthesized by *Bacillus siamensis* isolated from traditional fermented food in Thailand, *Int. J. Food Sci.* 2020 (2020), <https://doi.org/10.1155/2020/7352484>.
- [40] J. Matías, J. González, L. Royano, R.A. Barrena, Analysis of sugars by liquid chromatography-mass spectrometry in Jerusalem artichoke tubers for bioethanol production optimization, *Biomass Bioenergy* 35 (2011) 2006–2012, <https://doi.org/10.1016/j.biombioe.2011.01.056>.
- [41] Á. González-Garcinuño, A. Taberero, G. Marcelo, V. Sebastián, M. Arruebo, J. Santamaría, E. Martín del Valle, Differences in Levan nanoparticles depending on their synthesis route: microbial vs cell-free systems, *Int. J. Biol. Macromol.* 137 (2019) 62–68, <https://doi.org/10.1016/j.ijbiomac.2019.06.128>.
- [42] C. Campa, A. Oust, G. Skjåk-Bræk, B.S. Paulsen, S. Paoletti, B.E. Christensen, S. Ballance, Determination of average degree of polymerisation and distribution of oligosaccharides in a partially acid-hydrolysed homopolysaccharide: a comparison of four experimental methods applied to mannan, *J. Chromatogr. A* 1026 (2004) 271–281, <https://doi.org/10.1016/j.chroma.2003.11.045>.
- [43] B. Kekez, G. Gogic-Cvijovic, D. Jakovljevic, V. Pavlovic, V. Beskoski, A. Popovic, M.M. Vrvic, V. Nikolic, Synthesis and characterization of a new type of Levan-graft-polystyrene copolymer, *Carbohydr. Polym.* 154 (2016) 20–29, <https://doi.org/10.1016/j.carbpol.2016.08.001>.
- [44] S. Manandhar, S. Vidhate, N. D'Souza, Water soluble Levan polysaccharide biopolymer electrospun fibers, *Carbohydr. Polym.* 78 (2009) 794–798, <https://doi.org/10.1016/j.carbpol.2009.06.023>.
- [45] W. Xu, Q. Liu, Y. Bai, S. Yu, T. Zhang, B. Jiang, W. Mu, Physicochemical properties of a high molecular weight Levan from *brenneria* sp. eni D312, *Int. J. Biol. Macromol.* 109 (2018) 810–818, <https://doi.org/10.1016/j.ijbiomac.2017.11.056>.
- [46] S.S. Stivala, W.S. Bahary, L.W. Long, J. Ehrlich, E. Newbrun, I.I. Levans, Light-scattering and sedimentation data of streptococcus salivarius Levan in water, *Biopolymers* 14 (1975) 1283–1292, <https://doi.org/10.1002/bip.1975.360140616>.
- [47] A.D. Sezer, H. Kazak Sarilmiser, E. Rayaman, A. Çevikbas, E.T. Öner, J. Akbuga, Development and characterization of vancomycin-loaded Levan-based microparticulate system for drug delivery, *Pharm. Dev. Technol.* 22 (2017) 627–634, <https://doi.org/10.3109/10837450.2015.1116564>.
- [48] F. Sima, E.C. Mutlu, M.S. Eroglu, L.E. Sima, N. Serban, C. Ristoscu, S.M. Petrescu, E.T. Oner, I.N. Mihailescu, Levan nanostructured thin films by MAPLE assembling, *Biomacromolecules* 12 (2011) 2251–2256, <https://doi.org/10.1021/bm200340b>.
- [49] S.S. Stivala, J. Kimura, L. Reich, Thermal degradation of Levan, *Thermochim. Acta* 50 (1981) 111–122, [https://doi.org/10.1016/0040-6031\(81\)85049-6](https://doi.org/10.1016/0040-6031(81)85049-6).
- [50] J.R. Barone, M. Medynets, Thermally processed Levan polymers, *Carbohydr. Polym.* 69 (2007) 554–561, <https://doi.org/10.1016/j.carbpol.2007.01.017>.
- [51] M.S. Bostan, E.C. Mutlu, H. Kazak, S. Sinan Keskin, E.T. Oner, M.S. Eroglu, Comprehensive characterization of chitosan/PEO/levan ternary blend films, *Carbohydr. Polym.* 102 (2014) 993–1000, <https://doi.org/10.1016/j.carbpol.2013.09.096>.
- [52] A. Poli, H. Kazak, B. Gürleyendag, G. Tommonaro, G. Pieretti, E.T. Öner, B. Nicolaus, High level synthesis of Levan by a novel *halomonas* species growing on defined media, *Carbohydr. Polym.* 78 (2009) 651–657, <https://doi.org/10.1016/j.carbpol.2009.05.031>.
- [53] O. Tayan, M.T. Yilmaz, E. Dertli, Partial characterization of a Levan type exopolysaccharide (EPS) produced by *leuconostoc mesenteroides* showing immunostimulatory and antioxidant activities, *Int. J. Biol. Macromol.* 136 (2019) 436–444, <https://doi.org/10.1016/j.ijbiomac.2019.06.078>.
- [54] T.R. Crompton, *Polymer Reference Book*, Smithers Rapra Press, Akron, 2006.
- [55] Y.I. Matveev, V.Y. Grinberg, V.B. Tolstoguzov, The plasticizing effect of water on proteins, polysaccharides and their mixtures Glassy state of biopolymers, food and seeds, *Food Hydrocoll.* 14 (2000) 425–437, [https://doi.org/10.1016/S0268-005X\(00\)00020-5](https://doi.org/10.1016/S0268-005X(00)00020-5).
- [56] V.B. Tolstoguzov, The importance of glassy biopolymer components in food, *Nahrung* 44 (2000) 76–84, [https://doi.org/10.1002/\(SICI\)1521-3803\(20000301\)44:2<76::AID-FOOD76>3.0.CO;2-D](https://doi.org/10.1002/(SICI)1521-3803(20000301)44:2<76::AID-FOOD76>3.0.CO;2-D).
- [57] J.E. Zimeri, J.L. Kokini, The effect of moisture content on the crystallinity and glass transition temperature of inulin, *Carbohydr. Polym.* 48 (2002) 299–304, [https://doi.org/10.1016/S0144-8617\(01\)00260-0](https://doi.org/10.1016/S0144-8617(01)00260-0).
- [58] S. Ebnasajjad, Surface and material characterization techniques, in: W. Andrew (Ed.), *Surface Treatment of Materials for Adhesive Bonding*, Second edition, 2014, pp. 39–75.
- [59] E.A. Turi, *Thermal Characterization of Polymeric Materials*, Academic Press, 1981.
- [60] K.P. Menard, N.R. Menard, Dynamic mechanical analysis in the analysis of polymers and rubbers, in: *Encyclopedia of Polymer Science and Technology*, Wiley, 2015, pp. 1–33, <https://doi.org/10.1002/0471440264.pst102.pub2>.
- [61] D. Dunsion, in: *Characterization of Polymers Using Dynamic Mechanical Analysis (DMA)*, EAD Laboratories, 2017, pp. 1–8.
- [62] K.P. Menard, *Dynamic Mechanical Analysis: A Practical Introduction*, CRC Press, 1999.
- [63] Y. Song, K. Joo, J.H. Seo, Evaluation of mechanical and thermal properties of hydroxyapatite-Levan composite bone graft, *Biotechnol. Bioprocess Eng.* 26 (2021) 201–207, <https://doi.org/10.1007/s12257-020-0094-6>.